



26 **ABSTRACT**

27

28 Type 1 diabetes (T1D) is characterized by the autoimmune destruction of insulin-producing  $\beta$   
29 cells and involves an interplay between  $\beta$  cells and cells of the innate and adaptive immune  
30 systems. We investigated the therapeutic potential of targeting 12-lipoxygenase (12-LOX),  
31 an enzyme implicated in inflammatory pathways in  $\beta$  cells and macrophages, using a mouse  
32 model in which the endogenous mouse *Alox15* gene is replaced by the human  
33 *ALOX12* gene. Our finding demonstrated that VLX-1005, a potent 12-LOX inhibitor,  
34 effectively delayed the onset of autoimmune diabetes in human gene replacement non-  
35 obese diabetic mice. By spatial proteomics analysis, VLX-1005 treatment resulted in marked  
36 reductions in infiltrating T and B cells and macrophages with accompanying increases in  
37 immune checkpoint molecule PD-L1, suggesting a shift towards an immune-suppressive  
38 microenvironment. RNA sequencing analysis of isolated islets and polarized proinflammatory  
39 macrophages revealed significant alteration of cytokine-responsive pathways and a  
40 reduction in interferon response after VLX-1005 treatment. Our studies demonstrated that  
41 the *ALOX12* human replacement gene mouse provides a platform for the preclinical  
42 evaluation of LOX inhibitors and supports VLX-1005 as an inhibitor of human 12-LOX that  
43 engages the enzymatic target and alters the inflammatory phenotypes of islets and  
44 macrophages to promote the delay of autoimmune diabetes.

45

## 46 INTRODUCTION

47           The pathogenesis of type 1 diabetes (T1D) involves a complex interplay between  
48 multiple cell types within the pancreatic islet, including innate immune cells (macrophages,  
49 dendritic cells), insulin-producing cells ( $\beta$  cells), and adaptive immune cells (T cells, B cells)  
50 (1). Although the disease has traditionally been viewed as arising from a primary defect in  
51 immune tolerance, an emerging perspective posits that environmental factors (such as  
52 viruses or other systemic inflammatory disorders) may aggravate an interaction between  
53 macrophages and  $\beta$  cells, facilitating oxidative and endoplasmic reticulum (ER) stress  
54 pathways in  $\beta$  cells (2–4). These pathways facilitate the generation of  $\beta$ -cell neoepitopes  
55 that then trigger adaptive autoimmunity (5, 6). Disease-modifying therapies—those that alter  
56 disease pathogenesis rather than correcting the underlying disease phenotypes—have  
57 largely focused on the adaptive immune system and seen some successes in clinical trials.  
58 For example, an anti-CD3 monoclonal antibody (teplizumab) that targets activated T cells  
59 has been shown to delay the onset of T1D by up to two years in subjects at high risk for the  
60 disease (7). Given the increasing appreciation of innate immune cells and  $\beta$  cells in early  
61 T1D pathogenesis, the identification of drugs targeting these cell types raises the possibility  
62 that combination therapeutic approaches may provide more durable outcomes.

63           The lipoxygenases (LOXs) encompass a family of enzymes involved in lipid  
64 metabolism that facilitates the oxygenation of polyunsaturated fatty acids to form  
65 eicosanoids, some of which are pro-inflammatory in nature (8). In the mouse, 12/15-LOX is  
66 encoded by the *Alox15* gene and is the primary active LOX present in macrophages and  $\beta$   
67 cells and produces the proinflammatory eicosanoid 12-hydroxyeicosatetraenoic acid (12-  
68 HETE) as a principal product from the substrate arachidonic acid (9). Whole-body deletion of  
69 *Alox15* on the autoimmune non-obese diabetic (NOD) mouse background results in almost  
70 complete protection against diabetes (10). Deletion of *Alox15* in either the innate immune  
71 myeloid cells (2) or in  $\beta$  cells (11) recapitulates the autoimmune diabetes protection seen in  
72 the whole-body deletion, emphasizing both the early role of these cell types in T1D and the  
73 importance of the 12/15-LOX pathway in disease pathogenesis. In these cell-specific

74 deletion models, islets exhibit marked reductions in invading pathogenic T cells (insulinitis), a  
75 finding reflecting the disease-modifying response. The molecular events tied to disease  
76 protection ostensibly emanate from reductions in oxidative and ER stress (and the resultant  
77 reduction in neoepitope formation and presentation) as well as from enhanced display of PD-  
78 L1 (an immune-suppressive checkpoint ligand) on the surface of myeloid cells and  $\beta$  cells (2,  
79 11).

80 In humans, the relevant LOX enzyme that produces 12-HETE is 12-LOX, encoded by  
81 the *ALOX12* gene. Like the mouse 12/15-LOX, human 12-LOX is present in residual insulin-  
82 positive cells in donors with T1D or in autoantibody-positive donors at risk for T1D (12)—a  
83 finding consistent with a potential role in promoting  $\beta$ -cell sensitivity to autoimmunity. A  
84 major challenge to using mice as a platform to test inhibitors is that human 12-LOX exhibits  
85 structurally distinct characteristics from mouse 12/15-LOX, thereby necessitating the  
86 development of different inhibitors that cannot be tested for efficacy in mice (13–15).  
87 Previously, VLX-1005 (also known as ML355) was described as a potent and selective  
88 inhibitor of human 12-LOX while also displaying a favorable half-maximal inhibitory  
89 concentration ( $IC_{50}$ ) and pharmacokinetic (PK) properties (16). VLX-1005 was shown to  
90 protect human islets in vitro against dysfunction caused by proinflammatory cytokines (17),  
91 but the lack of appropriate in vivo model systems has made it challenging to  
92 pharmacologically validate VLX-1005 as a therapeutic target in autoimmune diabetes. To  
93 address this challenge, we developed new mouse strains in which the mouse *Alox15* gene is  
94 replaced by the human *ALOX12* gene while retaining the mouse gene's upstream control  
95 elements. This human gene replacement platform was leveraged to test if and how human  
96 12-LOX pharmacologic inhibition of human 12-LOX with VLX-1005 modifies disease  
97 progression in autoimmune T1D.

98

## 99 **RESULTS**

### 100 ***Generation and validation of the hALOX12 gene replacement mouse model***

101 To establish a platform to test potential inhibitors of human 12-LOX in vivo, we  
102 generated a mouse model in which the endogenous mouse *Alox15* gene is replaced by the  
103 human *ALOX12* gene (**Figure 1A**). This model leaves the mouse upstream regulatory region  
104 intact to ensure that the expression of *ALOX12* recapitulates the expression of *Alox15*.  
105 These mice (henceforth referred to as *hALOX12* mice) were introgressed onto the *C57BL/6J*  
106 mouse background using a speed congenics approach and bred to homozygosity.  
107 Microsatellite genotyping showed that the mice were 100% congenic on the *C57BL/6J* (or  
108 simply *B6*) background (**Supplemental Table 1** Excel file). To confirm the successful  
109 deletion of mouse *Alox15* and replacement with human *ALOX12*, we performed standard  
110 genotyping (**Supplemental Figure 1A**). Additionally, we isolated tissues (kidney, spleen,  
111 lung, fat, liver, islets, peritoneal macrophages, and bone marrow-derived macrophages  
112 (BMDMs)) from wildtype *B6* and *B6.hALOX12* mice and subjected them to gene expression  
113 analysis for *Alox15* and *ALOX12*. As anticipated, wildtype tissues expressed mouse *Alox15*  
114 and did not express human *ALOX12*; conversely, *B6.hALOX12* mice tissues expressed  
115 *ALOX12* but not *Alox15* (**Table 1**).

116 Because lipoxygenases are known to affect metabolic function, we next performed  
117 metabolic characterization to determine if/how the replacement of *Alox15* with *ALOX12*  
118 altered metabolic phenotypes. We found no significant differences in body weight, lean  
119 mass, fat mass, random-fed blood glucose levels, or glucose tolerance between wildtype *B6*  
120 and *B6.hALOX12* mice (**Supplemental Figure 1B-F**). Moreover, islet ultrastructure (relative  
121 immunostaining patterns of  $\alpha$  cells and  $\beta$  cells) and composition ( $\alpha$  cell mass and  $\beta$  cell  
122 mass) were indistinguishable between 10 week-old wildtype and *B6.hALOX12* mice  
123 (**Supplemental Figure 1G-I**). Taken together, these data suggest that the successful  
124 replacement of *Alox15* with human *ALOX12* did not alter gross metabolic or islet  
125 phenotypes.

126

127 ***Effects of VLX-1005 against STZ-induced diabetes are specific to B6.hALOX12 mice***

128 Prior studies demonstrated that whole-body deletion of mouse *Alox15* protects  
129 against diabetes induced by the chemical streptozotocin (STZ) (18). To test if the human 12-  
130 LOX inhibitor VLX-1005 (14) (**Figure 1B**) phenocopies deletion of the enzyme in our human  
131 gene replacement mice, we employed a similar STZ diabetes induction protocol. STZ is a  $\beta$   
132 cell toxin that induces low-grade inflammation, macrophage influx into islets, and eventual  
133 diabetes in mice after 5 daily low-dose intraperitoneal injections (55 mg/kg) (19). Eight-week-  
134 old male wildtype *B6* and *B6.hALOX12* mice were injected intraperitoneally daily with vehicle  
135 or 30 mg/kg VLX-1005 in the peri-STZ treatment period (for the 5 days before, during, and  
136 after STZ). STZ-injected *B6* and *B6.hALOX12* mice receiving vehicle became overtly  
137 hyperglycemic within 10 days of starting STZ treatment and displayed equivalent glucose  
138 intolerance by GTT (**Figure 1C and D**). Upon receiving VLX-1005, however, *B6.hALOX12*  
139 mice showed complete protection from STZ-induced diabetes, whereas wildtype *B6* mice  
140 became overtly hyperglycemic (**Figure 1E**); GTTs at the end of the study confirmed  
141 improved glucose tolerance in *B6.hALOX12* mice compared to wildtype *B6* mice (**Figure 1F**  
142 **and G**). These data indicate a specific effect of the drug in preventing hyperglycemia in  
143 *B6.hALOX12* mice and support the effectiveness of the *hALOX12* platform for interrogating  
144 VLX-1005 action.

145

#### 146 ***Pharmacokinetics of oral VLX-1005 and its effects on STZ-induced diabetes***

147 Given that the oral route is the preferred route for systemic drug delivery in humans,  
148 we next asked if oral administration of VLX-1005 provides adequate exposure in mice. We  
149 performed pharmacokinetic analysis following a single oral administration (as a suspension  
150 in 0.5% methylcellulose) of VLX-1005 spray dried dispersion at a dose of 30 mg/kg in  
151 C57BL/6J mice, followed by serial analysis of VLX-1005 levels by LC-MS/MS. The  
152 pharmacokinetic profile of orally-administered VLX-1005 in mice shows a mean half-life ( $T_{1/2}$ )  
153 of  $3.24 \pm 0.07$  hours and a consistent  $T_{max}$  of 0.250 hours across all mice. The  $C_{max}$  was  
154  $13300 \pm 624$  ng/ml, with moderate variability in AUC ( $15029 \pm 3177$  h\*ng/ml). These  
155 parameters, particularly the low variability in  $T_{max}$  and  $C_{max}$ , support the feasibility of once-

156 daily dosing for maintaining therapeutic levels over a 24-hour period (**Table 2**). We next  
157 tested the effects of oral administration of VLX-1005 on the low-dose STZ model, with VLX-  
158 1005 (at 30 mg/kg) given 3 days prior to the start of STZ, during STZ, and for 3 days  
159 following STZ treatment. Similar to intraperitoneal delivery, oral administration of VLX-1005  
160 in *B6.hALOX12* mice resulted in lower random-fed blood glucose levels (**Figure 1H**) and  
161 significantly improved glucose tolerance (**Figure 1I and J**) compared to vehicle—although  
162 this effect was not as robust as with intraperitoneal delivery of the drug. Consistent with  
163 improved glucose homeostasis, oral VLX-1005-treated mice exhibited greater  $\beta$  cell mass at  
164 the end of the study compared to vehicle-treated mice (**Figure 1K**). Collectively, these data  
165 suggest that a single daily oral delivery of VLX-1005 (at 30 mg/kg) achieves plasma levels  
166 with therapeutic efficacy.

167

#### 168 ***VLX-1005 treatment reduces $\beta$ cell inflammation in *NOD.hALOX12* mice***

169 The non-obese diabetic (*NOD*) mouse model is a model of T1D that recapitulates  
170 many of the immune and  $\beta$  cell features of the disease (20). We, therefore, asked if  
171 pharmacologic inhibition of 12-LOX using orally administered VLX-1005 protects against  
172 spontaneous diabetes development in the *NOD* mouse model. To address this question, we  
173 introgressed humanized *hALOX12* mice onto the *NOD* background using a speed congenics  
174 approach. Genome scanning of microsatellites was performed to confirm that mice were  
175 100% congenic on the *NOD* mouse background (*NOD.hALOX12* mice) (**Supplemental**  
176 **Table 1** Excel file). We next measured human 12-LOX protein levels in the *NOD.hALOX12*  
177 mice. Similar to the gene profile we observed in *B6.ALOX12* mice compared to wildtype  
178 *C57BL/6J* mice, wildtype *NOD* tissues robustly expressed mouse 12/15-LOX (the protein  
179 encoded by mouse *Alox15*) and little/no human *ALOX12*; conversely, *NOD.hALOX12* mice  
180 tissues robustly expressed human 12-LOX and minimal levels of 12/15-LOX (**Supplemental**  
181 **Figure 1J and 1K**). Consistent with their congenic nature, female *NOD.hALOX12* mice  
182 exhibited islet pathology similar to *NOD* mice at the (prediabetic) age of 10 weeks with  
183 evidence of T and B cell infiltration of islets (**Supplemental Figure 1L**) and indistinguishable

184 insulinitis score (**Supplemental Figure 1M**), suggesting that replacement of *Alox15* with  
185 human *ALOX12* did not alter the islet pathology of the disease. Pharmacokinetics of orally  
186 administered VLX-1005 (30 mg/kg) on the *NOD* background were similar to those seen in  
187 *C57BL/6J* mice (**Table 2**), suggesting that the *NOD* background does not affect drug  
188 absorption or clearance.

189 To assess the effect of VLX-1005 administration on products of 12-LOX activity in  
190 *NOD.hALOX12* mice, we administered 30 mg/kg VLX-1005 (or vehicle) orally to female  
191 *NOD.hALOX12* mice for 1 week during the pre-diabetic phase (8 weeks of age) and  
192 harvested serum. Lipidomics analysis (by LC/MS/MS) was performed for a series of 12-LOX  
193 products resulting from different fatty acid substrates (**Figure 2A**). Notably, levels of 12-  
194 HETE (from arachidonic acid), 13-HODE (from linoleic acid), and 14-HDHA and 17-HDHA  
195 (from docosahexaenoic acid) were all significantly reduced (**Figure 2B**). Levels of 12-HEPE  
196 (from eicosapentaenoic acid) were not significantly changed (**Figure 2B**), suggesting  
197 minimal involvement of eicosapentaenoic acid metabolism in *NOD* mice. Lipids within the  
198 pathway that are processed by enzymes other than 12-LOX were not statistically  
199 significantly altered (**Supplemental Table 2**). These data are collectively consistent with the  
200 expected 12-LOX engagement by VLX-1005.

201 To assess the effect of VLX-1005 administration on immune cell phenotypes in  
202 *NOD.hALOX12* mice, we administered 30 mg/kg VLX-1005 (or vehicle) orally to female  
203 *NOD.hALOX12* mice for 4 weeks during the pre-diabetic phase (6-10 weeks of age) and  
204 harvested pancreas, pancreatic lymph nodes (pLNs), and spleen (**Figure 2C**). Pancreas  
205 pathology showed reduced T and B cell infiltration and that the extent of insulinitis (by insulinitis  
206 scoring) was significantly reduced in VLX-1005-treated *NOD.hALOX12* mice compared to  
207 vehicle-treated mice (**Figure 2D-E**). To specifically interrogate the nature of immune cells  
208 within the insulitic region, we performed spatial tissue-based proteomics (Nanostring®). We  
209 used insulin immunostaining and nuclei staining to identify  $\beta$  cells and the surrounding  
210 insulitic regions. Pre-validated antibodies in the GeoMx® mouse immune panel were used to  
211 probe for immune cell subtypes in the peri-islet insulitic region and within the islet.



212 *NOD.hALOX12* mice exhibited a notable reduction of myeloid population subtypes in both  
213 insulitic and islet areas, including macrophages (F4/80+; CD11b+) and dendritic cells  
214 (CD11c+) (**Figure 2F** and **Supplemental Figure 2A-B**). This reduction in myeloid cell  
215 populations was accompanied by a decrease in T and B cells populations, including CD4+,  
216 CD3+, CD8+, and CD19+ cells (**Figure 2F** and **Supplemental Figure 2A-B**).  
217 Immunohistochemistry of pancreas sections confirmed the reductions in both T cells (CD3+),  
218 macrophages (F4/80+), and activated macrophages (Mac2+) following oral VLX-1005  
219 treatment (**Figure 2G**). A notable observation in spatial proteomics was the increased levels  
220 of the immune checkpoint ligand PD-L1 (**Figure 2F**). Enhanced PD-L1/PD-1 interactions  
221 shift T cells to less aggressive, more regulatory phenotypes (21). To interrogate this  
222 possibility, we performed immune profiling by flow cytometry of pancreatic lymph nodes  
223 (pLNs) from mice treated with oral VLX-1005 or vehicle. pLNs are key sites in the initial  
224 priming of autoreactive T cells in *NOD* mice (22). Treatment with oral VLX-1005 led to an  
225 increase in CD4+Foxp3+ regulatory T cells (Tregs) in the pLNs (**Supplemental Figure 2C**).  
226 This effect on Tregs was specific for the pLNs since no changes in Tregs were observed in  
227 the spleen after VLX-1005 treatment (**Supplemental Figure 2D**).

228

### 229 ***Orally-administered VLX-1005 reduces autoimmune diabetes incidence in female and*** 230 ***male NOD.hALOX12 mice***

231 Because 4 weeks of oral VLX-1005 dosing led to improvements in insulinitis and  
232 reductions in infiltrating T and B cells, we next asked if these alterations lead to prevention or  
233 delay of subsequent diabetes development in *NOD.hALOX12* mice. Both female and male  
234 mice were administered VLX-1005 via daily oral gavage (30 mg/kg) or vehicle for 4 weeks  
235 during the pre-diabetic phase (6-10 weeks of age). Mice were followed for diabetes  
236 development (blood glucose  $\geq 250$  mg/dl on 2 consecutive days) until 25 weeks of age  
237 (**Figure 3A**). At 25 weeks of age, 60% of female mice and 75% of male mice receiving VLX-  
238 1005 were protected from diabetes development compared to 25% of female and 50% of  
239 male mice receiving vehicle (**Figure 3B-C**). Whereas the preceding studies demonstrate that

240 12-LOX inhibition with oral VLX-1005 delays the development of diabetes, they do not  
241 address if administration of the drug might reverse established diabetes or mitigate  
242 hyperglycemia. We allowed female *NOD.hALOX12* mice to develop diabetes (defined as 2  
243 consecutive random-fed blood glucose measurements  $\geq 250$  mg/dL), then administered VLX-  
244 1005 or vehicle for up to 6 weeks via daily oral gavage or until the mice exhibited signs of  
245 physical deterioration from hyperglycemia (loss in body weight, dishevelment) (**Figure 3D**).  
246 Notably, we did not observe a reversal in diabetes but did see relative reductions in blood  
247 glucose levels in mice treated with VLX-1005 compared to vehicle (**Figure 3E-F**).

248

### 249 ***Orally-administered VLX-1005 reduces islet death and oxidative stress in***

#### 250 ***NOD.hALOX12 mice***

251 12-LOX is primarily present in islets and macrophages, and deletion of the mouse  
252 gene (*Alox15*) in either tissue separately was previously shown to reduce diabetes  
253 incidence. We, therefore, first asked how treatment with VLX-1005 affects islet cell  
254 phenotypes. We first subjected isolated islets from female *NOD.hALOX12* mice treated with  
255 vehicle or VLX-1005 to RNA sequencing to identify how islet gene expression might be  
256 altered. Principal component analysis of transcriptomics revealed that islets from vehicle-  
257 and VLX-1005-treated *NOD.hALOX12* mice clustered separately, suggesting an effect of  
258 VLX-1005 treatment on gene expression (**Figure 4A**). Pairwise comparison of gene  
259 expression using a false discovery rate (FDR) $<0.05$  and fold-change (FC) $>2$  yielded only  
260 189 differentially expressed genes. Instead, a  $P<0.05$  cutoff and  $FC>2$  revealed alteration of  
261 709 genes between vehicle- and VLX-1005-treated *NOD.hALOX12* mice (**Figure 4B**,  
262 volcano plot and **Supplemental Table 3** Excel file for full sequencing results). Gene  
263 Ontology pathway analysis showed significantly altered pathways related to DNA replication  
264 (e.g. *Anp32b*, *Skp1a*, *Itfg2*, *Dmrt1i*), inflammation (NF $\kappa$ B activity) (e.g. *Elf1*, *Trim75*, *RNase1*,  
265 *Lmo1*, *Bcl3*, *Ptgis*, *Commd1*, *Lrrc14*, *Foxp3*), and G-protein coupled receptor signaling (e.g.  
266 *Gpr89*, *Glp2r*), among others (**Figure 4C**). These pathways suggest responses that may be  
267 related to changes in cellular survival in response to VLX-1005. We, therefore,

268 immunostained pancreatic sections for markers of cell death and proliferation in the islet.  
269 VLX-1005-treated *NOD.hALOX12* mice exhibited decreased islet cell death as measured by  
270 reduced terminal deoxynucleotidyl transferase dUTP nick end labeling (TUNEL) and H2A  
271 histone family member X (H2A.X) staining compared to vehicle-treated mice (**Figure 4D**).  
272 Additionally, VLX-1005-treated mice demonstrated decreased  $\beta$  cell proliferation, as  
273 measured by proliferating cell nuclear antigen (PCNA) immunostaining (**Figure 4D**); reduced  
274 PCNA immunostaining was also consistent with the reduction of Ki67 observed in spatial  
275 proteomics of the insulin+ area (**Figure 2F** and **Supplemental Figure 2B**). We interpret the  
276 reduction in  $\beta$  cell proliferation as a consequence of reduced  $\beta$  cell apoptosis. The alteration  
277 in NF $\kappa$ B signaling led us to investigate if markers of oxidative stress were affected since  
278 inflammation, oxidative stress, and  $\beta$  cell survival are closely linked (23, 24). We performed  
279 immunostaining for the oxidative stress marker, 4-hydroxynonenal (4-HNE) and observed  
280 reduced immunostaining in mice treated with VLX-1005 compared to placebo (**Figure 4E**).  
281 Consistent with this observation,  $\beta$  cells from VLX-1005-treated animals also displayed an  
282 increase in levels of the antioxidant enzyme GPx1 (**Figure 4E**). Collectively, these data are  
283 consistent with prior observed effects of reduced inflammation, oxidative stress, and  $\beta$  cell  
284 death in  $\beta$  cell-specific deletion of mouse *Alox15* in NOD mice (11).

285

### 286 ***VLX-1005 alters the proinflammatory macrophage phenotype***

287       Whereas the preceding findings are consistent with improved  $\beta$  cell survival following  
288 oral VLX-1005 administration, these studies do not rule out the possibility that the drug  
289 directly modifies the phenotype of infiltrating macrophages, which could secondarily affect  $\beta$   
290 cells. Because bulk islet transcriptomics analysis does not resolve gene expression events  
291 associated with specific cell types, we isolated bone marrow-derived macrophages (BMDMs)  
292 from female *NOD.hALOX12* mice and then performed RNA sequencing in the presence or  
293 absence of VLX-1005. BMDMs were unpolarized (“M0”) or polarized to an “M1-like” state  
294 (with lipopolysaccharide and IFN- $\gamma$ ) to mimic the inflammatory state that might be observed  
295 during T1D pathogenesis. During polarization, BMDMs were treated with vehicle or VLX-

296 1005 (**Figure 5A**). Principal component analysis of transcriptomics revealed that M0  
297 macrophages treated with VLX-1005 co-clustered with vehicle-treated M0 macrophages,  
298 suggesting a minimal transcriptional effect of the drug on unpolarized cells (**Figure 5B**).  
299 Consistent with this interpretation, only 1% of genes (159 out of 15,888) were significantly  
300 altered with VLX-1005 treatment (when using criteria  $FC > 2$  and  $P < 0.05$ ) (**Supplemental**  
301 **Table 4** Excel file for full sequencing results). Upon polarization to the M1-like state, a clear  
302 rightward shift in the principal component analysis plot was observed with both vehicle and  
303 VLX-1005-treated BMDMs and a notable separation was seen between vehicle and VLX-  
304 1005 treatment (**Figure 5B**); this finding suggests that the impact of 12-LOX inhibition is  
305 more prominent upon a shift to a proinflammatory state of macrophages.

306 We next interrogated the gene expression events associated with the M0 to M1  
307 transition in both vehicle and VLX-1005-treated BMDMs. Most genes altered ( $FC > 2$  and  
308  $P < 0.05$ ) in this transition (2467) were common between vehicle and VLX-1005 treatment  
309 (**Figure 5C-D**, **Supplemental Figure 3A**, and **Supplemental Table 4** Excel file). These  
310 common genes mapped to pathways related to cytokine-mediated signaling, T cell  
311 activation, and antigen processing and presentation (**Supplemental Figure 3B**). An  
312 additional 507 genes were significantly altered in vehicle-treated cells, and 459 additional  
313 genes were significantly altered with VLX-1005 treatment (**Supplemental Figure 3A**). The  
314 507 genes altered with vehicle treatment mapped to GO pathways related to the M1  
315 polarization phenotype (myeloid cell differentiation, immune response, response to  
316 cytokines) and pathways related to oxidative stress (cell redox homeostasis, response to  
317 hydrogen peroxides) (**Figure 5E**). These pathways were not identified in the genes that were  
318 differentially expressed during VLX-1005 treatment. GO pathway analysis of the 459 genes  
319 altered with VLX-1005 showed particularly significant alterations in pathways related to  
320 modification of the interferon response (**Figure 5F**). Next, we looked specifically at the genes  
321 that mapped to interferon pathways (**Figure 5G**), which revealed that VLX-1005 augmented  
322 significantly ( $P < 0.05$  by T-test) the magnitude of the gene changes compared to vehicle  
323 treatment. Notable genes, whose directional changes are known to counter the interferon

324 response included *Oas1e* (25), *Till12* (26), and *Adar* (27) (all upregulated compared to  
325 control-treated M1 macrophages), and *Gigyf2* (28) and *Mmp12* (29) (correspondingly  
326 downregulated) (**Figure 5G**). These data suggest effects of VLX-1005 that may lead to  
327 reduced macrophage interferon signaling.

328

329

## 330 **DISCUSSION**

331 To date, the adaptive immune system has remained the primary focus for the  
332 development of therapeutics aimed at preventing or reversing T1D. Notwithstanding the  
333 utility of agents such as anti-CD3 monoclonal antibodies in preserving  $\beta$  cell function (30) or  
334 delaying T1D development (7), there has been impetus in the research community to  
335 develop therapeutics that target other cell types that contribute to T1D development (31),  
336 including innate immune cells and  $\beta$  cells. A multi-targeted approach is expected to aid in  
337 better disease modification and result in more durable and broadly applicable therapy (32).  
338 In this respect, 12/15-LOX (in mice) is a particularly appealing target since it is active in both  
339 macrophages and  $\beta$  cells and contributes to the development of inflammatory disorders,  
340 including insulin resistance, atherosclerosis, and T1D (for review, see (9)). The deletion of  
341 *Alox15*, specifically in either myeloid cells or islet  $\beta$  cells, proved sufficient to delay/prevent  
342 T1D in NOD mice (2, 11). Evidence for 12-LOX contributions to T1D pathogenesis identifies  
343 this enzyme as an attractive target in human disease. 12-LOX is elevated in  $\beta$  cells of  
344 autoantibody-positive, pre-T1D individuals and in residual  $\beta$  cells of individuals with  
345 established T1D (12). A pro-inflammatory product derived from the 12-LOX (and mouse  
346 12/15-LOX)-mediated metabolism of arachidonic acid is 12-HETE, an eicosanoid that either  
347 directly or indirectly (through G-protein-coupled receptors (33–36)) augments reactive  
348 oxygen species generation and endoplasmic reticulum stress in macrophages and islets (37,  
349 38). Notably, levels of 12-HETE were shown to be elevated in the circulation of youth and  
350 adults with new-onset T1D (compared to healthy controls and those with established T1D)  
351 (39).

352 Considering the biological contributions of the 12-LOX enzymes (mouse 12/15-LOX  
353 and human 12-LOX) to T1D and other inflammatory disorders, the development of enzyme  
354 inhibitors offers an attractive approach to disease modification. Inhibition of 12/15-LOX using  
355 ML351 demonstrated promising outcomes in NOD mice, with reductions in insulinitis and  
356 improvements in glucose homeostasis (13). An inhibitor that showed mouse and human  
357 cross-species reactivity, ML127, unfortunately also displayed evidence of off-target

358 cytotoxicity (13). By contrast, VLX-1005 (a.k.a. ML355) is a potent inhibitor ( $IC_{50}$  ~300 nM) of  
359 human 12-LOX (14) that has shown efficacy in reversing the insulin secretory defects of  
360 cytokine-treated human islets in vitro without evidence of cytotoxicity (17); however, the  
361 benefit of this inhibitor in disease states in vivo has remained speculative. To address the  
362 translational challenge of testing 12-LOX inhibitors in preclinical disease models in vivo, we  
363 developed a human gene replacement mouse model on both the C57BL/6J and NOD  
364 autoimmune diabetes backgrounds. The utility of this model as a platform for 12-LOX  
365 inhibitor testing was confirmed in our multiple low-dose STZ studies, which showed that  
366 VLX-1005 administration to *B6.ALOX12* mice precluded hyperglycemia, whereas wild-type  
367 controls developed hyperglycemia over time. STZ is a toxin whose full effects involve  
368 communication between  $\beta$  cells and macrophages (19), and our findings with systemic  
369 administration of VLX-1005 are consistent with similar STZ studies in mice harboring the  
370 global deletion of *Alox15* (18)—collectively suggesting that human *ALOX12* gene  
371 replacement mice respond appropriately to a 12-LOX inhibitor and that the human *ALOX12*  
372 gene can sufficiently replace the functionality of the mouse *Alox15* gene.

373         In recent studies, our group showed that loss of the mouse *Alox15* gene in either  
374 myeloid cells or islet  $\beta$  cells could protect animals from the development of autoimmune  
375 diabetes on the NOD background (2, 11). The pathological phenotypes of these animals  
376 were similar, with reductions in islet invasion by T cells, B cells, and myeloid cells and a  
377 characteristic increase in PD-L1 in either macrophages or  $\beta$  cells. PD-L1 is an immune  
378 checkpoint protein whose interaction with its receptor PD-1 on adaptive immune cells leads  
379 to a more immune-suppressive response (21). In our studies using *NOD.ALOX12* mice, we  
380 found similar responses to VLX-1005 treatment, with striking reductions in both innate and  
381 adaptive immune cell infiltration into the islets and a notable increase in PD-L1 in the insulitic  
382 (immune cell) component. We interpret these latter findings to suggest that the effect of  
383 systemically administered VLX-1005 may be greater in macrophages than in  $\beta$  cells. The  
384 reductions in markers of  $\beta$  cell proliferation, death, and oxidative stress that we observed  
385 with VLX-1005 treatment may also be reflective of this preferential effect on macrophages

386 since these responses are otherwise characteristic of the effects of cytokines on  $\beta$  cells (40).  
387 Our RNA-Seq studies of isolated NOD mouse BMDMs polarized to the proinflammatory M1  
388 state support this contention, as VLX-1005 treatment resulted in reductions in the interferon  
389 response. Our studies open the possibility that VLX-1005 may be useful in autoimmune  
390 diabetes resulting from PD-L1 or PD-1 blockade (checkpoint inhibitor therapy) often used to  
391 treat cancers (41).

392 Some limitations to our study should be acknowledged. First, because our mouse  
393 model replaces the mouse *Alox15* with the human *ALOX12* globally, we cannot be certain  
394 that the effects we observed are exclusively related to the inhibition of the human enzyme in  
395 only macrophages and  $\beta$  cells; a recent study suggested that mouse *Alox15* may contribute  
396 to pro-resolving functions of Tregs (42). It remains unclear, therefore, if the loss of *Alox15*  
397 globally in our mouse model might have affected Treg function or the function of other cell  
398 types that have low levels of *Alox15* expression. In this respect, our mouse model may have  
399 limited utility in other disease states where *ALOX12* might not fully replace the function of  
400 *Alox15*. Moreover, we cannot rule out the possibility that *Alox15* and *ALOX12* mediate  
401 distinct pathways that nevertheless still allow for shared phenotypes. For example, our RNA  
402 sequencing studies of macrophages treated with VLX-1005 reveal distinct reductions in  
403 interferon-mediated responses but such effects have not been directly explored as a  
404 consequence of *Alox15* in mice. Second, our studies do not fully address the timing and  
405 duration of VLX-1005 treatment. We only treated mice for a 4-week period (6-10 weeks of  
406 age); it is possible that a longer duration of treatment might have yielded even more robust  
407 T1D prevention outcomes. Therefore, the timing and duration of human treatment may  
408 require further investigation in our preclinical model. Limitations regarding timing and  
409 duration may also apply to diabetes “reversal” studies, in which we observed a reduction in  
410 glycemia but no reversal in disease. We cannot rule out the possibility that the effect of VLX-  
411 1005 to suppress  $\beta$  cell proliferation may have prevented a more robust outcome in this  
412 case. Finally, our study does not assess the potential for 12-LOX inhibition in combination  
413 with other immunomodulatory agents. Whereas the relatively modest impact of VLX-1005



414 treatment in the diabetes reversal studies in *NOD.ALOX12* mice might suggest diminishing  
415 returns on the treatment of humans at the time of disease diagnosis, this effect may be  
416 amplified in the presence of T or B cell blockade.

417         Despite these limitations, our studies identify a new platform on which to study a  
418 class of LOX inhibitors for their utility in ameliorating human autoimmune diabetes. Our  
419 human gene replacement mouse model demonstrates a functional equivalence between  
420 mouse *Alox15* and human *ALOX12* in the context of T1D since the whole-body replacement  
421 of the mouse gene with the human (under the mouse upstream control elements) preserves  
422 islet pathology and the frequency of diabetes incidence in NOD mice. Therefore, beyond its  
423 utility to test inhibitors of human 12-LOX, our mouse model also provides a platform to  
424 interrogate the cause-effect relationship of human 12-LOX in T1D and possibly other  
425 inflammatory diseases in vivo.

426

427 **MATERIALS and METHODS**

428

429 ***Sex as a biological variable***

430 For *C57BL/6J* mice, our study examined only male mice, because comparative data  
431 for these mice in the literature are primarily from males. For *NOD* mice, our study mostly  
432 examined females, because type 1 diabetes in the *NOD* strain is more frequently observed  
433 in females. However, some data from *NOD* male mice are included that parallel those seen  
434 in females, suggesting that the effects observed in females may be relevant to males.

435

436 ***Animals***

437 Male and female *C57BL/6J* mice and *NOD/ShiLTJ* mice were procured from the  
438 Jackson Laboratory. All mice were kept under pathogen free housing conditions with  
439 standard light:dark (12:12 h) cycles and fed ad lib normal chow. To generate a humanized  
440 *ALOX12* mouse model, the coding region of the mouse *Alox15* gene was replaced with the  
441 coding region of the human *ALOX12* gene while retaining all the mouse regulatory elements  
442 (**Figure 1A**) (mice were generated by a contract to Ingenious Targeting Laboratory).  
443 Targeted iTL BF1 (*C57BL/6* FLP) embryonic stem cells were microinjected into *Balb/c*  
444 blastocysts. Chimeras with high percentage of black coat color resulting from this procedure  
445 were then mated to *C57BL/6J* wildtype mice to generate germline neo-deleted mice. The  
446 following primers were used to genotype the mice: 5'-  
447 TCTGATCTGTGTATGCCTGTGTGTGG-3' (forward) and 5'-  
448 TTCCAAGGAAAAAGGCATGGTTTCTGAGG-3' (reverse). These primers generate a 478 bp  
449 band for wildtype and 581 bp band for knock-in mice (**Supplemental Figure 1A**).

450 Human *ALOX12* alleles were introgressed onto both the *C57BL/6J* and *NOD.ShilT/J*  
451 mouse backgrounds using a speed congenics approach based on microsatellite genotyping  
452 at The Jackson Laboratory. Genome scanning was also performed at The Jackson  
453 Laboratory to confirm successful backcrossing onto the *C57BL/6J* and *NOD.ShilT/J* mouse

454 background (*B6.hALOX12* and *NOD.hALOX12*; **Supplemental Table 1** excel file). Body  
455 mass was measured by EchoMRI.

456 Intraperitoneal glucose tolerance tests (IPGTT) were performed in mice after  
457 overnight fasting (16 h). Mice were intraperitoneally injected with glucose at a dose of 1 or 2  
458 g/kg body weight and blood glucose levels were measured at specific time points: 0, 10, 20,  
459 30, 60, 90, and 120 minutes after glucose injection using an AlphaTrak glucometer.

460

#### 461 ***Formulation of VLX-1005***

462 VLX-1005 was obtained from Veralox Therapeutics Inc (Frederick, MD). A VLX-1005  
463 spray-dried dispersion (for oral administration) was prepared by dissolving VLX-1005 and  
464 HPMC-E3 in a 90:10 w/w mixture of tetrahydrofuran and water to attain a total solids  
465 concentration of 5% w/w. 1575 g of solution was then spray dried using a Buchi B-290  
466 laboratory spray dryer. The yield after spray drying was 67.8 g. The collected material was  
467 further dried in an oven at 40 °C under vacuum to remove residual tetrahydrofuran.

468

#### 469 ***Pharmacokinetic Analysis and Lipidomics***

470 Following intraperitoneal injection or oral gavage, VLX-1005 was quantified in plasma  
471 using high-performance liquid chromatography-tandem mass spectrometry (Triple Quad  
472 6500+; Sciex) after separation by HPLC (Column: Agilent Poroshell 120 EC-C18; HPLC:  
473 Shimadzu DGU-405). Pharmacokinetic parameters for VLX-1005 were estimated by non-  
474 compartmental model using WinNonlin 8.3. The bioavailability (F%) was calculated as the  
475 following:  $AUC_{last}^{PO}/AUC_{INF}^{PO} > 80\%$ :  $F = (AUC_{INF}^{PO} * Dose_{IV}) / (mean AUC_{INF}^{IV} * Dose_{PO})$ . Lipidomics on serum samples was performed by the New York Medical  
477 College Lipidomics Core using a Shimadzu LC-MS/MS 8050 system equipped with a  
478 UHPLC and auto-sampler.

479

#### 480 ***Streptozotocin (STZ) Induction***

481 Male *C57BL/6J* and *B6.hALOX12* mice (8-10 weeks of age) were injected with either  
482 vehicle (0.5% methylcellulose) or 30 mg/kg/day of VLX-1005 by intraperitoneal injection for  
483 15 days: 5 days prior to the start of multiple low-dose STZ (55 mg/kg/day; 5 consecutive  
484 days), 5 days during STZ treatment, and 5 days post STZ injections. Male *B6.hALOX12*  
485 mice (8-10 weeks of age) were injected with either vehicle (0.5% methylcellulose) or 30  
486 mg/kg/day of VLX-1005 by oral gavage (PO) for 11 days: 3 days prior to the start of multiple  
487 low dose STZ (55 mg/kg/day; 5 consecutive days), 5 days during STZ treatment, and 3 days  
488 post STZ injections. Random-fed glucose levels were measured by tail snip using a  
489 glucometer (AlphaTrak), and mice were followed for 20 days post-STZ injections. IPGTT  
490 was performed on day 4 post-STZ treatments after overnight fasting. At the end of each  
491 study, mice were euthanized, and pancreas and blood samples were collected.

492

#### 493 ***Diabetes Incidence and Treatment***

494 Both male and female *NOD.hALOX12* mice were given either vehicle or 30  
495 mg/kg/day VLX-1005 (PO) for 4 weeks in the pre-diabetic stage (6-10 weeks of age) and  
496 then followed for diabetes incidence until 25 weeks of age or until diabetes diagnosis.  
497 Diabetes incidence was determined by observing two consecutive blood glucose values  
498 greater than 250 mg/dL. At the end of each study, mice were euthanized, and pancreas and  
499 blood samples were collected.

500 For diabetes treatment studies, female *NOD.hALOX12* mice were followed for  
501 random-fed blood glucose from 12-20 weeks of age. At diabetes incidence (two consecutive  
502 blood glucose values greater than 250 mg/dL), mice were administered 30 mg/kg/day VLX-  
503 1005 SDD or vehicle for up to 6 weeks via daily oral gavage or until the mice exhibited signs  
504 of physical deterioration from hyperglycemia (loss in body weight, dishevelment). At the end  
505 of each study, mice were euthanized, and pancreas and blood samples were collected.

506

#### 507 ***Islet and Macrophage Isolation***

508 Islets were isolated from *NOD.hALOX12* mice with either vehicle or 30 mg/kg/day of  
509 VLX-1005 treatment using collagenase digestion. Briefly, collagenase was injected into the  
510 pancreatic bile duct to digest the connective tissue and release pancreatic cells (43). A  
511 Histopaque-HBSS gradient was applied to the dissociated pancreas and centrifuged at 900  
512 xg for 18 min. The isolated islets were cultured in RPMI medium. The collected islets were  
513 handpicked and allowed to recover overnight before processing. RNA was isolated for use in  
514 RNA sequencing or quantitative PCR.

515 Bone marrow-derived macrophages (BMDMs) were isolated from 8-week-old  
516 *NOD.hALOX12* mice as described previously (2). The isolated BMDMs were cultured for 7  
517 days in complete medium (RPMI containing 10% FBS, 10 mM HEPES, and 100 U/ml  
518 penicillin/ streptomycin) supplemented with 10 ng/ml M-CSF. On day 7 of culture, the  
519 BMDMs were pretreated with either vehicle (0.1% DMSO) or 10  $\mu$ M VLX-1005. After 1 h  
520 pretreatment, the BMDMs were further stimulated with 10 ng/ml LPS and 25 ng/mL IFN- $\gamma$  for  
521 18 h for M1-like polarization. RNA was isolated and used for sequencing.

522

### 523 ***RNA Isolation and Quantitative PCR***

524 RNA was isolated from mouse tissues and macrophages using an RNeasy Mini® Kit  
525 from Qiagen. The isolated RNA was used to synthesize cDNA using a High-Capacity cDNA  
526 Reverse Transcription kit (Applied Biosystems) according to manufacturer's instructions.  
527 Quantitative PCR was performed using a Bio-Rad CFX Opus with a predesigned Taqman®  
528 assay probe for human and mouse genes: human *ALOX12*: Hs00167524\_m1; mouse  
529 *Alox15*: Mm00507789\_m1; mouse *Actb*: Mm01205647\_m1 (Invitrogen). The relative gene  
530 expression levels were calculated using the comparative threshold cycle value (Ct) and  
531 normalized to *Actb*.

532

### 533 ***Immunostaining, $\beta$ Cell Mass, and Insulinitis Scoring***

534 Pancreatic tissues were fixed using 4% paraformaldehyde. After fixation, the tissues  
535 were embedded in paraffin and sectioned with a thickness of 5  $\mu$ m. Three sections per

536 mouse were used for analysis, with each section being spaced 100  $\mu\text{m}$  apart. Tissue  
537 sections were immunostained with anti-insulin (ProteinTech; 15848-1-AP; 1:200), anti-  
538 glucagon (Abcam; ab92517; 1:200), anti-12-LOX (Thermo Fisher; PA5-26020; 1:200), anti-  
539 12/15-LOX (Abcam; ab80221; 1:200), anti-CD3 (Abcam; ab16669; 1:200), anti-F4/80  
540 (Sigma; D2S9R; 1:150), anti-MAC2 (Thermo Fisher; EbioM3/38; 1:200) and anti-H2A.X (Cell  
541 Signaling Technology; 9718s; 1:200) primary antibodies followed by conjugated anti-rabbit Ig  
542 (Vector Laboratories) secondary antibody. A DAB (3,3'-diaminobenzidine) Peroxidase  
543 Substrate Kit from Vector Laboratories was used for detection. After immunostaining, the  
544 tissue sections were counterstained with hematoxylin (Sigma). Images were acquired using  
545 a BZ-X810 fluorescence microscope (Keyence) and  $\beta/\alpha$  cell mass was quantified by insulin+  
546 or glucagon+ area and whole pancreas area. Insulinitis score reflects the degree of immune  
547 cell infiltration within pancreatic islets. The score system used as follow: 1 = no insulinitis, 2 =  
548 infiltrate <50% circumference, 3 = infiltrate >50% circumference, 4 = infiltration within islet.  
549 Data are shown as the average insulinitis score per mouse.

550 For immunofluorescence staining, pancreatic sections were stained with the following  
551 antibodies: anti-insulin (Dako IR002; 1:4), anti-glucagon (Santa Cruz; sc514592; 1:50), anti-  
552 B220 (Biolegend; 03201; 1:100), anti-CD3 (Abcam; ab16669; 1:200), anti-PCNA (Santa  
553 Cruz; sc-7907; 1:100), anti-4HNE (Abcam; ab46545; 1:200), and anti-GPx1 (Santa Cruz; sc-  
554 22145; 1:100). Highly cross-adsorbed Alexa Fluor secondary antibodies (ThermoFisher)  
555 were used at a dilution of 1:500. Tissue sections were stained with DAPI (ThermoFisher) to  
556 label cell nuclei. The Nikon A1 confocal microscopy was used to capture images. CellProfiler  
557 v4.1 software was used for image analysis.

558

### 559 ***TUNEL Staining***

560 Terminal deoxynucleotidyl transferase dUTP nick end labelling (TUNEL) assay was  
561 used to determine  $\beta$  cell death in pancreatic islets. The assay was performed according to  
562 the protocol provided by the manufacturer (Abcam) and HRP-DAB chemistry was used for  
563 detection. Two sections, spaced 100  $\mu\text{m}$  apart, were used for each mouse. Images were

564 captured using a BZ-X810 fluorescence microscope system (Keyence). The number of  
565 TUNEL+ cells was assessed manually per islet.

566

### 567 ***NanoString Spatial Proteomics***

568 Paraffin embedded pancreata were used for NanoString spatial proteomics analysis.  
569 Tissues were stained with morphology markers: AF-647 conjugated insulin (Cell Signaling;  
570 9008s; 1:400) and nuclei marker (SYTO13). Tissues were hybridized using a pre-validated  
571 mouse GeoMx Immune cell panel (NanoString; GMX-PROCONCT-MICP) comprising of the  
572 following markers: PD-1, CD11c, CD8a, PanCk, MHC II, CD19, CTLA4, SMA, CD11b,  
573 CD3e, Fibronectin, Ki-67, CD4, GZMB, F4/80, CD45, PD-L1; housekeeping genes: Histone  
574 H3, S6, GAPDH; and IgG antibodies: Rb IgG, Rat IgG2a, and Rat IgG2b for background  
575 subtraction. All markers were conjugated to unique UV-photocleavable oligos for indexing. At  
576 least 5-6 islets with insulinitis were chosen as regions of interest (ROI) per mouse based on  
577 the morphology markers (insulin and nuclei). The ROIs were segmented into insulitic region  
578 and insulin+ region for each islet. Oligos from the segmented ROIs were photocleaved,  
579 collected in a 96-well plate, and reads were counted using nCounter (NanoString). Scaling  
580 was performed to normalize for any differences in tissue surface area and depth. After  
581 scaling, reads were normalized to housekeeping markers and background was subtracted  
582 using IgG markers.

583

### 584 ***Flow Cytometry***

585 Spleen and pancreatic lymph nodes were harvested, homogenized, and passed  
586 through a 70  $\mu\text{m}$  strainer to obtain a single cell suspension. Cell pellets were resuspended in  
587 red blood cell (RBC) lysing solution to remove red blood cells.  $2.5 \times 10^5$ -  $1 \times 10^6$  cells per  
588 condition were incubated with blocking solution (eBioscience; 14-0161-86) containing anti-  
589 mouse CD16/CD32 to block the Fc receptors for 20 min on ice. The following surface  
590 markers were used — CD4- FITC (BioLegend; 100510; 1:100), CD8-PerCP-Cy5.5  
591 (Biolegend; 100734; 1:100), CD19-AF700 (Biolegend; 152414; 1:100). Following incubation

592 of surface antibodies, cells were washed with stain buffer and then permeabilized using  
593 fix/perm buffer (BD #554722) before intracellular staining. The following intracellular  
594 antibodies were used FoxP3-AF647 (BD; 560401; 1:100), IFN $\gamma$ -PE (BD; 554412; 1:50), and  
595 IL17a-APCCY7 (BD; 560821; 1:50). Cells were analyzed on the Attune NxT Flow Cytometer  
596 (Thermo Fisher). Data were analyzed by FlowJo software (BD Biosciences).

597

### 598 ***RNA Sequencing***

599 RNA extraction was performed using RLT Buffer, according to the manufacturer's  
600 instructions (Qiagen). Samples were submitted for library generation and sequencing by the  
601 University of Chicago sequencing core using a NovaSeq 6000<sup>®</sup> (Illumina). Data was  
602 analyzed using Galaxy (<https://usegalaxy.org/>). Reads were aligned to the Mus musculus  
603 genome build mm10 using HISAT2. Individual sample reads were quantified using HTseq-  
604 count and normalized using DESeq2. DESeq2 was also used to calculate fold changes and  
605 P-values and to perform optional covariate correction. Gene ontology (GO) was used for  
606 pathway analysis.

607

### 608 ***Statistical Methods***

609 All data are represented as mean  $\pm$  SEM. When comparing more than two  
610 conditions, one-way ANOVA was performed. Tukey's post-hoc test or Dunnett's post-hoc  
611 test was used to determine specific differences between individual group means. When  
612 comparing only two conditions, two-tailed student's t-test was performed. Mantel-Cox log-  
613 rank test was specifically used for analyzing the NOD diabetes incidence experiments. Data  
614 analyses were performed using the GraphPad Prism 10 software. The differences were  
615 considered statistically significant at a p value <0.05.

616

### 617 ***Study Approval***



618 All experiments involving mice were performed at the University of Chicago and the  
619 procedures were conducted according to protocols approved by the University of Chicago  
620 Institutional Animal Care and Use Committee (Chicago, IL).

621

622 ***Data Availability***

623 The islet RNA sequencing data have been uploaded to the Gene Expression  
624 Omnibus (<https://www.ncbi.nlm.nih.gov/geo/>) with accession number GSE272668. The  
625 BMDM sequencing data have been uploaded to the Gene Expression Omnibus with  
626 accession number GSE272687. Values for all data points in graphs are reported in the  
627 Supporting Data Values file.

628

629

630 **ACKNOWLEDGEMENTS**

631 This work was supported in part by National Institutes of Health grants R03  
632 TR003381 (to SAT and RGM), R41 DK122917 (to RGM and DJM), R01 DK10558 (to RGM),  
633 U01 DK127786 (to RGM), T32 AI153020 (to JRE), an investigator-initiated award from  
634 Veralox Therapeutics (to SAT and RGM), a Chicago Biomedical Consortium Director's  
635 Award (to RGM), and Breakthrough T1D postdoctoral fellowship (3-PDF-2023-1326-A-N)  
636 and Diabetes Research Connection awards (both to CM). This study utilized Diabetes  
637 Center core resources supported by National Institutes of Health grant P30 DK020595 (to  
638 the University of Chicago) and utilized services of the University of Chicago Histology and  
639 Genomics Cores.

640

641 **AUTHOR CONTRIBUTIONS**

642 JLN, DJM, MBB, SAT, and RGM conceptualized the research; TN, CM, JRE, JEW,  
643 AC, KF, SP, JBN, and SAT performed investigation; SAT and RGM provided project  
644 supervision; TN, SCM, SAT, and RGM wrote the original draft; all authors contributed to  
645 discussion, edited the manuscript, and approved the final version of the manuscript.

646

647 **DECLARATION OF INTERESTS**

648 RGM and SAT received an investigator-initiated award from Veralox Therapeutics.  
649 RGM serves on the Scientific Advisory Board for Veralox Therapeutics. DJM and MBB are  
650 Veralox Therapeutics employees.

651 **REFERENCES**

652

653 1. Atkinson MA, Mirmira RG. The pathogenic “symphony” in type 1 diabetes: A disorder of  
654 the immune system,  $\beta$  cells, and exocrine pancreas. *Cell Metab.* 2023;S1550-  
655 4131(23)00228–0.

656

657 2. Kulkarni A, et al. 12-Lipoxygenase governs the innate immune pathogenesis of islet  
inflammation and autoimmune diabetes. *JCI Insight.* 2021;6(14):147812.

658

659 3. Lee H, et al. Beta Cell Dedifferentiation Induced by IRE1 $\alpha$  Deletion Prevents Type 1  
Diabetes. *Cell Metab.* 2020;31(4):822-836.e5.

660

661 4. Tersey SA, et al. Islet  $\beta$ -cell endoplasmic reticulum stress precedes the onset of type 1  
diabetes in the nonobese diabetic mouse model. *Diabetes.* 2012;61(4):818–827.

662

663 5. Gonzalez-Duque S, et al. Conventional and Neo-antigenic Peptides Presented by  $\beta$  Cells  
664 Are Targeted by Circulating Naïve CD8+ T Cells in Type 1 Diabetic and Healthy Donors. *Cell  
Metab.* 2018;28(6):946-960.e6.

665

666 6. Roep BO, et al. Type 1 diabetes mellitus as a disease of the  $\beta$ -cell (do not blame the  
immune system?). *Nat Rev Endocrinol.* 2021;17(3):150–161.

667

668 7. Herold KC, et al. An Anti-CD3 Antibody, Teplizumab, in Relatives at Risk for Type 1  
Diabetes. *N Engl J Med.* 2019;381(7):603–613.

669

670 8. Dobrian AD, et al. Functional and pathological roles of the 12- and 15-lipoxygenases.  
*Prog Lipid Res.* 2011;50:115–131.

671

672 9. Kulkarni A, et al. Regulation of Tissue Inflammation by 12-Lipoxygenases. *Biomolecules.*  
2021;11(5):717.

673

674 10. McDuffie M, et al. Nonobese diabetic (NOD) mice congenic for a targeted deletion of  
675 12/15-lipoxygenase are protected from autoimmune diabetes. *Diabetes.* 2008;57(1):199–  
208.

676

677 11. Piñeros AR, et al. Proinflammatory signaling in islet  $\beta$  cells propagates invasion of  
pathogenic immune cells in autoimmune diabetes. *Cell Rep.* 2022;39(13):111011.

678

679 12. Grzesik WJ, et al. Expression pattern of 12-lipoxygenase in human islets with type 1  
diabetes and type 2 diabetes. *J Clin Endocrinol Metab.* 2015;100(3):E387-395.

680

681 13. Hernandez-Perez M, et al. Inhibition of 12/15-Lipoxygenase Protects Against  $\beta$ -Cell  
682 Oxidative Stress and Glycemic Deterioration in Mouse Models of Type 1 Diabetes. *Diabetes.*  
2017;66(11):2875–2887.

683

684 14. Luci D, et al. Discovery of ML355, a Potent and Selective Inhibitor of Human 12-  
685 Lipoxygenase. *Probe Reports from the NIH Molecular Libraries Program.* Bethesda (MD):  
National Center for Biotechnology Information (US); 2010.

686

687 15. Rai G, et al. Discovery of ML351, a Potent and Selective Inhibitor of Human 15-  
688 Lipoxygenase-1. *Probe Reports from the NIH Molecular Libraries Program.* Bethesda (MD):  
National Center for Biotechnology Information (US); 2010.

- 689 16. Luci DK, et al. Synthesis and structure-activity relationship studies of 4-((2-hydroxy-3-  
690 methoxybenzyl)amino)benzenesulfonamide derivatives as potent and selective inhibitors of  
691 12-lipoxygenase. *J Med Chem*. 2014;57(2):495–506.
- 692 17. Ma K, et al. 12-Lipoxygenase Inhibitor Improves Functions of Cytokine-Treated Human  
693 Islets and Type 2 Diabetic Islets. *J Clin Endocrinol Metab*. 2017;102(8):2789–2797.
- 694 18. Bleich D, et al. Resistance to type 1 diabetes induction in 12-lipoxygenase knockout  
695 mice. *J Clin Invest*. 1999;103:1431–1436.
- 696 19. Calderon B, et al. Dendritic cells in islets of Langerhans constitutively present beta cell-  
697 derived peptides bound to their class II MHC molecules. *Proc Natl Acad Sci U S A*.  
698 2008;105(16):6121–6126.
- 699 20. Anderson MS, Bluestone JA. The NOD mouse: a model of immune dysregulation. *Annu*  
700 *Rev Immunol*. 2005;23:447–485.
- 701 21. Falcone M, Fousteri G. Role of the PD-1/PD-L1 Dyad in the Maintenance of Pancreatic  
702 Immune Tolerance for Prevention of Type 1 Diabetes. *Front Endocrinol (Lausanne)*.  
703 2020;11:569.
- 704 22. Gagnerault M-C, et al. Pancreatic Lymph Nodes Are Required for Priming of  $\beta$  Cell  
705 Reactive T Cells in NOD Mice. *Journal of Experimental Medicine*. 2002;196(3):369–377.
- 706 23. Evans-Molina C, et al. PPAR- $\gamma$  Activation Restores Islet Function in Diabetic  
707 Mice Through Reduction of ER Stress and Maintenance of Euchromatin Structure. *Mol Cell*  
708 *Biol*. 2009;29:2053–2067.
- 709 24. Tersey SA, et al. 12-Lipoxygenase Promotes Obesity-Induced Oxidative Stress in  
710 Pancreatic Islets. *Mol Cell Biol*. 2014;34(19):3735–3745.
- 711 25. Harioudh MK, et al. The canonical antiviral protein oligoadenylate synthetase 1 elicits  
712 antibacterial functions by enhancing IRF1 translation. *Immunity*. 2024;57(8):1812-1827.e7.
- 713 26. Ju L-G, et al. TLL12 Inhibits the Activation of Cellular Antiviral Signaling through  
714 Interaction with VISA/MAVS. *J Immunol*. 2017;198(3):1274–1284.
- 715 27. Knebel UE, et al. Disrupted RNA editing in beta cells mimics early-stage type 1 diabetes.  
716 *Cell Metab*. 2024;36(1):48-61.e6.
- 717 28. Xu Z, et al. SARS-CoV-2 impairs interferon production via NSP2-induced repression of  
718 mRNA translation. *Proc Natl Acad Sci U S A*. 2022;119(32):e2204539119.
- 719 29. Dufour A, et al. C-terminal truncation of IFN- $\gamma$  inhibits proinflammatory macrophage  
720 responses and is deficient in autoimmune disease. *Nat Commun*. 2018;9(1):2416.
- 721 30. Herold KC, et al. Anti-CD3 monoclonal antibody in new-onset type 1 diabetes mellitus. *N*  
722 *Engl J Med*. 2002;346:1692–1698.
- 723 31. von Herrath M, et al. Anti-interleukin-21 antibody and liraglutide for the preservation of  $\beta$ -  
724 cell function in adults with recent-onset type 1 diabetes: a randomised, double-blind,  
725 placebo-controlled, phase 2 trial. *Lancet Diabetes Endocrinol*. 2021;9(4):212–224.
- 726 32. Long SA, Speake C. Combination therapy in recent-onset type 1 diabetes. *Lancet*  
727 *Diabetes Endocrinol*. 2021;9(4):191–193.

- 728 33. Ermis E, et al. Leukotriene B4 receptor 2 governs macrophage migration during tissue  
729 inflammation. *J Biol Chem*. 2024;300(1):105561.
- 730 34. Guo Y, et al. Identification of the orphan G protein-coupled receptor GPR31 as a  
731 receptor for 12-(S)-hydroxyicosatetraenoic acid. *J Biol Chem*. 2011;286:33832–33840.
- 732 35. Hernandez-Perez M, et al. A 12-lipoxygenase-Gpr31 signaling axis is required for  
733 pancreatic organogenesis in the zebrafish. *FASEB J*. 2020;34(11):14850–14862.
- 734 36. Yokomizo T, et al. Hydroxyeicosanoids bind to and activate the low affinity leukotriene  
735 B4 receptor, BLT2. *J Biol Chem*. 2001;276(15):12454–12459.
- 736 37. Chen M, et al. Activation of 12-lipoxygenase in proinflammatory cytokine-mediated beta  
737 cell toxicity. *Diabetologia*. 2005;48:486–495.
- 738 38. Weaver JR, et al. Integration of pro-inflammatory cytokines, 12-lipoxygenase and NOX-1  
739 in pancreatic islet beta cell dysfunction. *Mol Cell Endocrinol*. 2012;358(1):88–95.
- 740 39. Hennessy E, et al. Elevated 12-hydroxyicosatetraenoic acid (12-HETE) levels in serum  
741 of individuals with newly diagnosed Type 1 diabetes. *Diabet Med*. 2017;34(2):292–294.
- 742 40. Eizirik DL, Colli ML, Ortis F. The role of inflammation in insulinitis and beta-cell loss in type  
743 1 diabetes. *Nat Rev Endocrinol*. 2009;5(4):219–226.
- 744 41. Chen X, et al. Immune Checkpoint Inhibitors and Risk of Type 1 Diabetes. *Diabetes*  
745 *Care*. 2022;45(5):1170–1176.
- 746 42. Marques RM, et al. Loss of 15-lipoxygenase disrupts Treg differentiation altering their  
747 pro-resolving functions. *Cell Death Differ*. 2021;28(11):3140–3160.
- 748 43. Stull ND, et al. Mouse islet of Langerhans isolation using a combination of purified  
749 collagenase and neutral protease. *J Vis Exp*. 2012;(67):4137.
- 750

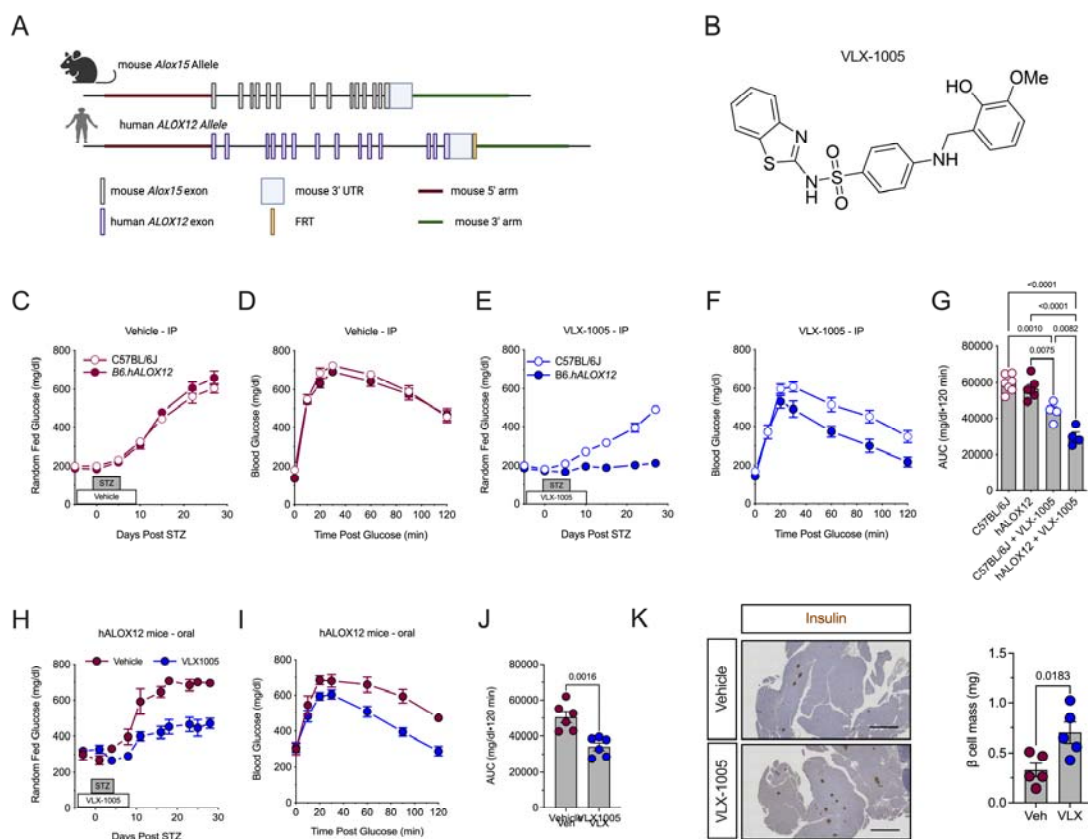
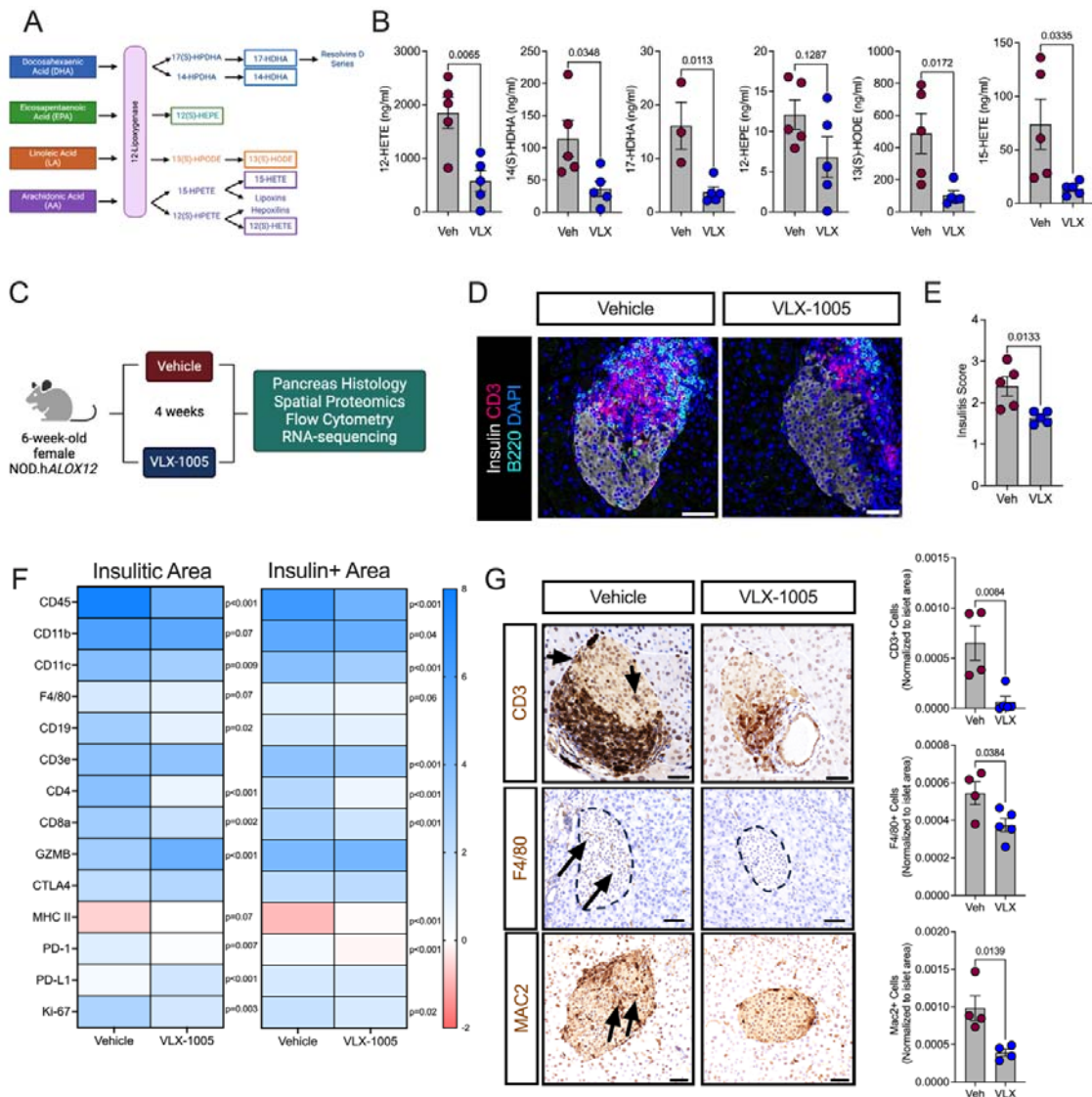


**Figure 1: 12-LOX inhibition protects against streptozotocin-induced diabetes.**

*C57BL/6J* and *B6.hALOX12* male mice (N=4-7 per group as indicated) were treated with 30 mg/kg intraperitoneal or PO VLX-1005 and multiple low-dose streptozotocin (STZ). (A) Schematic of the generation of *hALOX12* mice by replacing mouse *Alox15* with human *ALOX12*. (B) Chemical structure of VLX-1005. (C) Random-fed blood glucose values in vehicle-treated male *C57BL/6J* and *B6.hALOX12* mice after STZ. (D) GTT of vehicle-treated male *C57BL/6J* and *B6.hALOX12* mice after STZ at day 4 post-STZ-treatment. (E) Random-fed blood glucose values in VLX-1005-treated male *C57BL/6J* and *B6.hALOX12* mice after STZ. (F) GTT of VLX-1005-treated male *C57BL/6J* and *B6.hALOX12* mice after STZ at day 4 post-STZ-treatment. (G) AUC of *C57BL/6J* and *B6.hALOX12* after STZ at day 4 post-STZ-treatment (one-way ANOVA). (H) Random-fed blood glucose values in male vehicle- or VLX-1005-treated (PO) *B6.hALOX12* mice after STZ. (I) GTT of male vehicle- or VLX-1005-treated (PO) *B6.hALOX12* mice after STZ at day 4 post-STZ-treatment. (J) AUC of *B6.hALOX12* after STZ at day 4 post-STZ-treatment. (K) Pancreata stained for insulin (left panel) and  $\beta$  cell mass measurement (right panel) from male *B6.hALOX12* mice at day 26 post-STZ-treatment. Scale bars = 500  $\mu$ m. Data are presented as mean  $\pm$ SEM and statistical significance was determined by a two-tailed T-test or one-way ANOVA.

751  
752  
753  
754  
755  
756  
757  
758  
759  
760  
761  
762  
763  
764  
765  
766  
767  
768  
769  
770



771

772

773

774 **Figure 2: VLX-1005 decreased islet inflammation in *NOD.hALOX12* female mice.** 6-

775 week-old female pre-diabetic *NOD.ALOX12* mice were treated orally with 30 mg/kg VLX-

776 1005 for 4 weeks prior to tissue analysis. (A) Schematic representation of 12-lipoxygenase

777 products. (B) Serum lipidomics results of 12-lipoxygenase products as indicated (N=4-5). (C)

778 Schematic representation of mouse treatment paradigm. (D) Pancreata from mice stained

779 for CD3 (magenta), B220 (teal), insulin (white), and nuclei (blue). Scale bars = 50 μm. (E)

780 Average insulinitis score, each dot represents an individual mouse (N=4-5). (F) Heatmap of

781 identified proteins in the insulitic area (left panel) and insulin-positive area (right panel). (G)

782 Pancreata of mice stained and quantified for CD3 (brown, top panels; arrows indicate

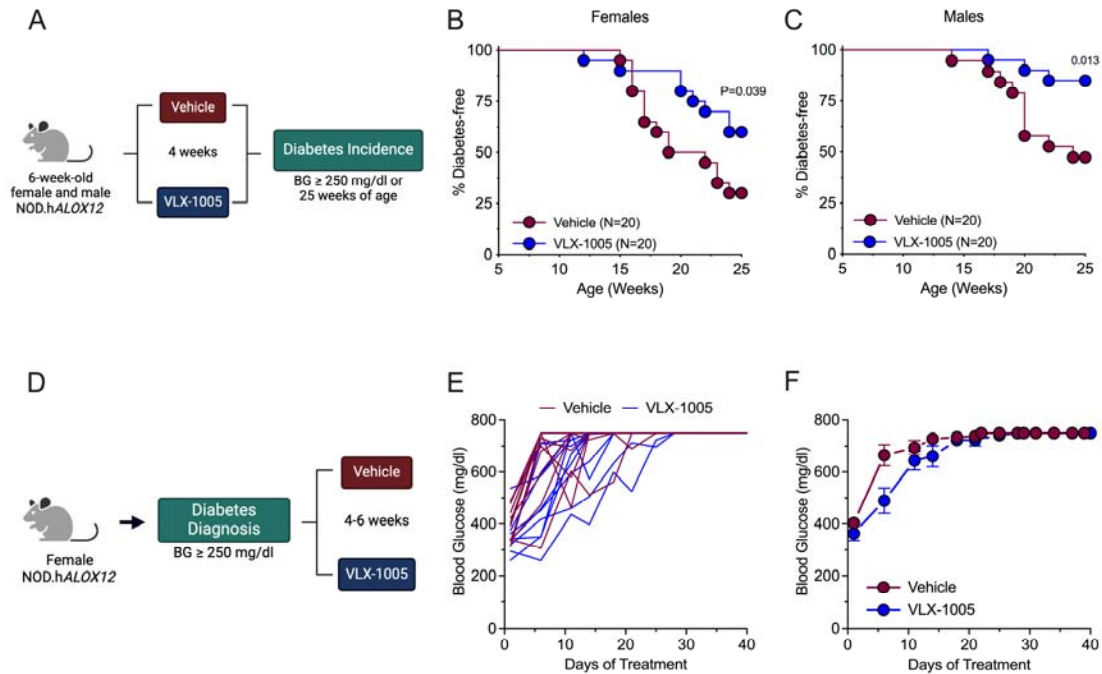
783 positive CD3 staining within the islet), F4/80 (brown, middle panels; arrows indicate positive

784 F4/80 staining within the islet), or MAC2 (brown, bottom panels; arrows indicate positive

785 MAC2 staining within the islet) and nuclei (blue). Each dot represents an individual mouse

786 (N=4-5). Scale bars = 50 μm. Data are presented as mean ± SEM and statistical significance

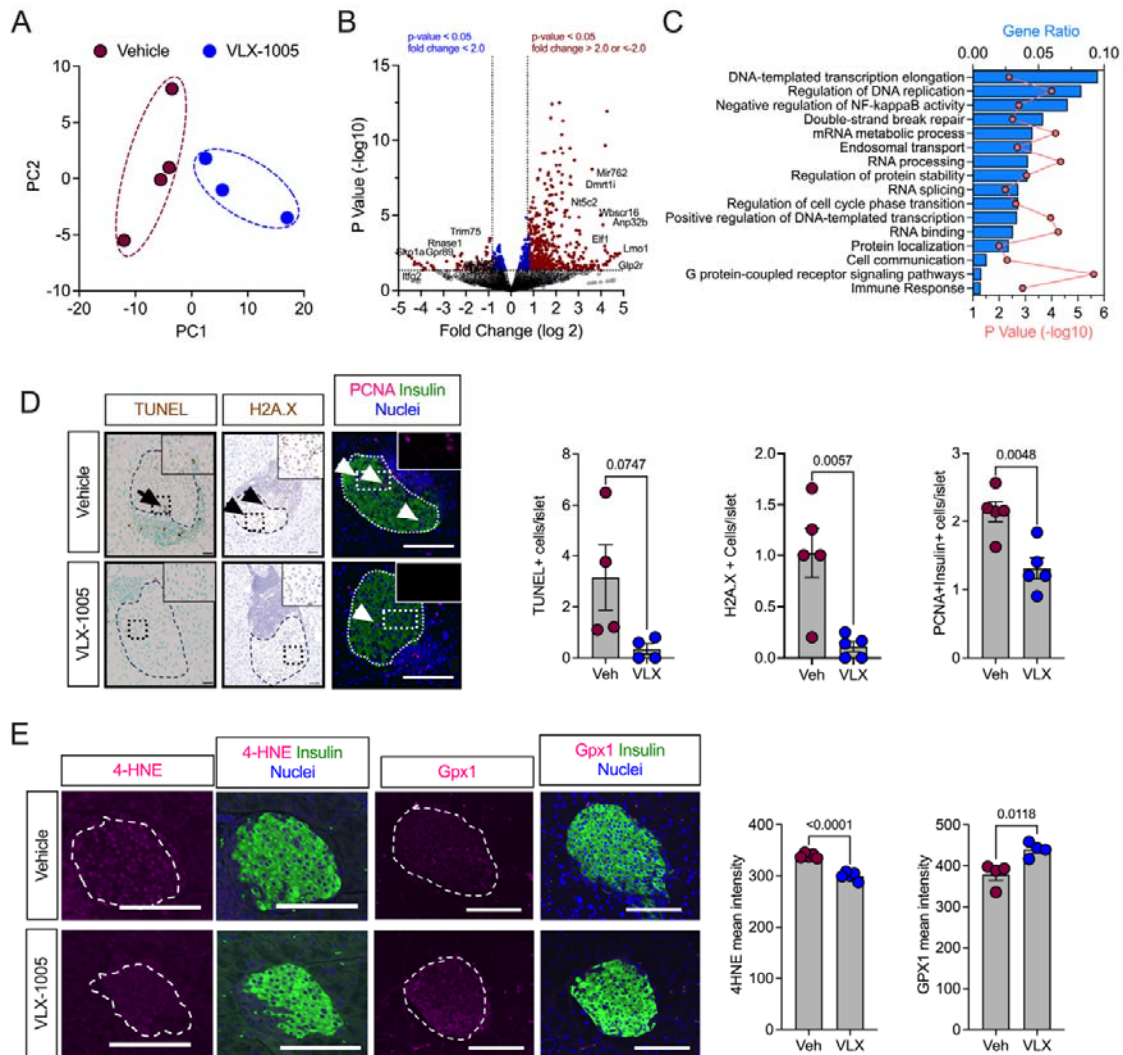
787 was determined by a two-tailed T-test in all cases.



788  
789  
790  
791  
792  
793  
794  
795  
796  
797  
798  
799

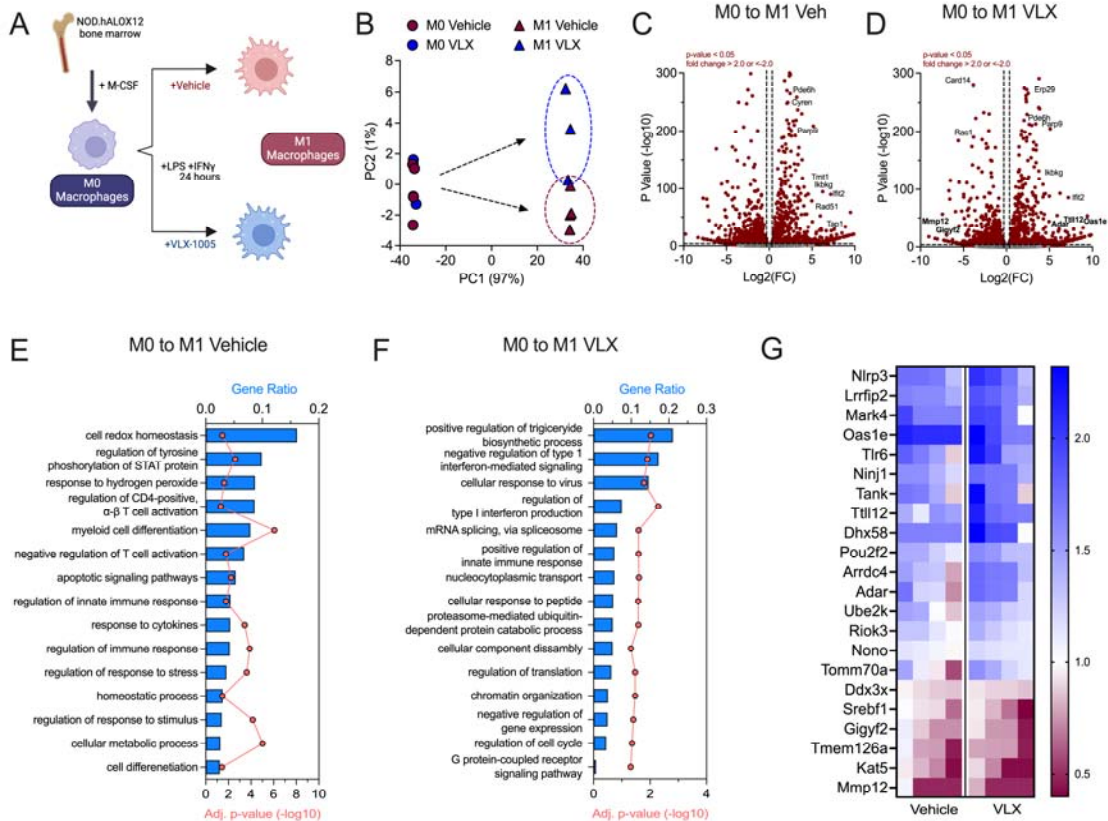
**Figure 3: VLX-1005 treatment delays autoimmune diabetes onset in female and male *NOD.hALOX12* mice.** *NOD.hALOX12* mice (N=20 per group) were treated during the pre-diabetic stage from 6-10 weeks of age or at the time of diabetes development (N=11-12 per group). **(A)** Schematic representation of diabetes prevention experimental design. **(B)** Diabetes incidence in female *NOD.hALOX12* mice. **(C)** Diabetes incidence in male *NOD.hALOX12* mice. **(D)** Schematic representation of diabetes reversal experimental design. **(E)** Random-fed blood glucose levels in each female mouse. **(F)** Average random-fed blood glucose levels of female mice. Data are presented as mean  $\pm$ SEM and statistical significance was determined by a Mantel-Cox Log Rank test.





800  
801  
802  
803  
804  
805  
806  
807  
808  
809  
810  
811  
812  
813  
814  
815  
816  
817

**Figure 4: VLX-1005 decreased  $\beta$  cell death, proliferation, and oxidative stress in female *NOD.hALOX12* mice.** Pancreata or islets were harvested from 10-week-old prediabetic female *NOD.hALOX12* mice after 4 weeks of treatment with vehicle or VLX-1005 (N=3-4 per group). **(A)** Principal component analysis plot of RNA-sequencing results from isolated islets of vehicle- or VLX-1005-treated mice. **(B)** Volcano plot of differentially expressed genes. **(C)** Gene ontology pathway analysis of differentially expressed genes. **(D)** Pancreata from mice stained and quantified for TUNEL (brown, *left panels*; black arrow indicates positive TUNEL staining within the islet), H2A.X (brown, *middle panels*; black arrowheads indicate positive H2A.X staining within the islet), or PCNA (magenta, *right panels*; white arrowheads indicate positive PCNA staining within the islet), insulin (green) and nuclei (blue). Each dot represents an individual mouse (N=4-5). Scale bars = 50  $\mu$ m. **(E)** Pancreata from mice stained and quantified for 4-HNE (magenta, *left panels*), or GPx1 (magenta, *right panels*), and insulin (green) and nuclei (blue). Each dot represents an individual mouse (N=4). Scale bars = 50  $\mu$ m. Data are presented as mean  $\pm$  SEM and statistical significance was determined by a two-tailed T-test.



818  
819  
820  
821  
822  
823  
824  
825  
826  
827  
828  
829  
830  
831  
832  
833

**Figure 5: RNA-sequencing analysis of M1-like bone marrow derived macrophages reveals a reduction in the inflammatory response upon VLX-1005 treatment.** Bone marrow-derived macrophages (BMDMs) were isolated and polarized to the M1-like state and treated with vehicle or VLX-1005 (10  $\mu$ M) during polarization. RNA was isolated and sequenced (N=4 per group). (A) Schematic of experimental design. (B) Principal component analysis plot. (C) Volcano plot of differentially expressed genes in M0 and M1-like vehicle-treated macrophages. (D) Volcano plot of differentially expressed genes in M0 and M1-like VLX-1005-treated macrophages. (E) Gene ontology pathway analysis of differentially expressed genes in M0 vs M1-like vehicle-treated macrophages. (F) Gene ontology pathway analysis of differentially expressed genes in M0 vs M1-like VLX-1005-treated macrophages. (G) Heatmap of significantly altered interferon-related genes. Columns represent sequencing results from each sample (N=4 per group). Numbers on the heatmap scale indicate fold change compared to M0 macrophages.

834 **Table 1: RNA expression levels of human *ALOX12* and mouse *Alox15* normalized to**  
 835 **mouse *Actb* from various isolated tissues of *C57BL/6J* and *B6.hALOX12* mice.**  
 836

| Mouse Strain              | Tissues                   | <i>ALOX12</i><br>( $\Delta$ CT) | <i>Alox15</i><br>( $\Delta$ CT) |
|---------------------------|---------------------------|---------------------------------|---------------------------------|
| <b><i>C57BL/6J</i></b>    | Islets                    | ND                              | 7.66 $\pm$ 0.32                 |
|                           | Spleen                    | ND                              | 18.41 $\pm$ 1.31                |
|                           | BMDM                      | ND                              | 17.47 $\pm$ 0.03                |
|                           | Peritoneal<br>Macrophages | ND                              | 3.62 $\pm$ 0.26                 |
|                           | Liver                     | ND                              | 12.2 $\pm$ 1.77                 |
|                           | Kidney                    | ND                              | 15.02 $\pm$ 0.09                |
|                           | Lung                      | ND                              | 9.65 $\pm$ .063                 |
|                           | Fat                       | ND                              | 10.84 $\pm$ 0.55                |
|                           | <b><i>B6.hALOX12</i></b>  | Islets                          | 7.91 $\pm$ 0.18                 |
| Spleen                    |                           | 14.11 $\pm$ 0.26                | ND                              |
| BMDM                      |                           | 14.48 $\pm$ 0.47                | ND                              |
| Peritoneal<br>Macrophages |                           | 6.06 $\pm$ 0.16                 | ND                              |
| Liver                     |                           | 13.88 $\pm$ 0.32                | ND                              |
| Kidney                    |                           | 10.12 $\pm$ 0.10                | ND                              |
| Lung                      |                           | 13.68 $\pm$ 0.32                | ND                              |
| Fat                       |                           | 8.05 $\pm$ 0.42                 | ND                              |

837 ND

=  
not  
det  
ect  
ed.

844 **Table 2: Plasma concentration vs time profile for VLX-1005 after 30 mg/kg PO in**  
 845 **C57BL/6J mice and NOD.ShiLt/J mice.**  
 846

| Pharmacokinetic Parameter       | C57BL/6J      |        | NOD.ShiLt/J   |        |
|---------------------------------|---------------|--------|---------------|--------|
|                                 | Mean ± SD     | CV (%) | Mean ± SD     | CV (%) |
| *T <sub>1/2</sub> (h)           | 3.24 ± 0.07   | 2.17   | 2.53 ± 0.41   | 16.1   |
| T <sub>max</sub> (h)            | 0.250 ± 0.00  | 0.00   | 0.250 ± 0.00  | 0.000  |
| C <sub>max</sub> (ng/ml)        | 13300 ± 624   | 4.70   | 14253 ± 5474  | 38.4   |
| AUC <sub>last</sub> (h*ng/ml)   | 15029 ± 3177  | 21.1   | 13211 ± 1631  | 12.3   |
| AUC <sub>inf</sub> (h*ng/ml)    | 15083 ± 3206  | 21.3   | 13225 ± 1625  | 12.3   |
| AUC <sub>%Extrap_obs</sub> (%)  | 0.342 ± 0.133 | 38.9   | 0.115 ± 0.099 | 85.6   |
| MRT <sub>inf_obs</sub> (h)      | 2.57 ± 0.38   | 14.8   | 3.81 ± 0.71   | 18.7   |
| AUC <sub>last/D</sub> (h*ng/ml) | 501 ± 106     | 21.1   | 440 ± 54      | 12.3   |

859  
 860 \*T<sub>1/2</sub>, half life; T<sub>max</sub>, time to maximum drug concentration; C<sub>max</sub>, maximum drug concentration; AUC<sub>last</sub>, area under  
 861 the curve from the time of dosing to the last measurable concentration; AUC<sub>inf</sub>, area under the curve from the  
 862 time of dosing extrapolated to infinity; AUC<sub>%extrap\_obs</sub>, area under the curve from the time of dosing extrapolated to  
 863 last observed concentration; MRT<sub>inf\_obs</sub>, mean residence time from the time of dosing extrapolated to infinity;  
 864 AUC<sub>last/D</sub>, dose normalized area under the curve to time of last measurable concentration.